Experimental section

Chemicals and materials

Copper(II) nitrate hydrate ($Cu(NO_3)_2 \cdot 3H_2O$, ≥ 99%), Cetyltrimethylammonium bromide (CTAB, ≥ 99%) and Hexamethylene tetramine (HMT, ≥ 95%) were obtained from Sinopharm Chem. Reagent Co. Ltd. Ethylene glycol ($C_2H_6O_2$, A. R. grade), Ethanol (C_2H_5OH, 99.7%), Isopropanol (C_3H_8O , A. R. grade), and Potassium hydroxide (KOH, 99.5%) were purchased from Shanghai Macklin Biochemical Technology Co., Ltd. Nano copper powder (60-100 nm, 99.9%) was sourced from Beijing Innokai Technology Co., Ltd. (Methyl sulfoxide)-d6 (DMSO-d6, ≥99.8% + TMS) was bought from Shanghai Titan Technology Co., Ltd. 5 wt% Nafion solution was obtained from Alfa Aesar. Anion exchange membrane (Fumasep FAB-PK-130) was obtained from Fuel Cell Store CO_2 gas (99.99%) and Ar gas (99.9%) were purchased from Wuxi Xin Xiyi Technology. Gas diffusion layer (GDL, 28BC) was obtained from SGL Group. Pt mesh (0.8 cm × 0.8 cm, 0.5 mm thickness) was custom-made from Shanghai Jing Chong Electronic Technology Development Co., Ltd. Silver chloride electrode (Ag/AgCl, CHI111) was purchased from Shanghai Yucai Electronic Technology Co., Ltd. All reagents were analysis reagent (A.R.), and used as received without further purification. Deionized water (Milli-Q) was used for the synthesis of nanomaterials.

Synthesis of CuO-nanoflowers

The above chemicals and materials are used directly without further purification. Initially, the mixture consisting of 2 mmol of $Cu(NO_3)_2 \cdot 3H_2O$ was dissolved in 50 mL of deionized water containing 10 mL of ethylene glycol, followed by the addition of 0.02 g of CTAB and 0.8 g of HMT. After sonication for 1 h, the homogeneous solution was transferred to a 100 mL autoclave and kept at 115°C for 4 h. After natural cooling to room temperature, the CuO was collected, washed several times with deionized water and ethanol and finally dried in a vacuum oven at 60°C for 8 hours.

Nano copper powder is used directly without further modification.

Preparation of electrodes

To prepare the cathode electrode, a catalyst ink that contained 10 mg of obtained

catalyst, 950 μL of isopropanol and 50 μL of Nafion ionomer solution was sonicated for 30 min. 50 μL of the ink was then loaded onto a 0.7 cm × 0.7 cm GDL to create a GDE. The mass loading of catalyst was controlled at 1mg cm^{-2} by adjusting the catalyst ink amount. Platinum mesh was used as the anode electrode when operated at alkaline electrolyte.

Electrochemical measurements

All electrochemical measurements were performed in a flow cell composed of a GDE, a anion exchange membrane and a platinum anode. The electrolysis was controlled by CS (CS310H, Wuhan Corrtest Instruments Corp., Ltd) electrochemical workstation. Saturated Ag/AgCl was used as the reference and it was calibrated with respect to RHE: E (RHE) = E (Ag/AgCl) + 0.0595 × PH + 0.223. All of the electrocatalytic reactions were conducted at ambient pressure and temperature.

1 M KOH aqueous solution was used as electrolyte and was circulated through the anode side using a peristaltic pump. High-purity CO_2 was supplied to the cathode with a digital gas flow controller. The outlet flowrate was measured by another digital flowmeter. The electrocatalytic CO_2RR measurements were carried out under the current density range from 100 mA cm^{-2} to 400 mA cm^{-2} to obtain the reduction products. During the electrolytic reaction, the effluent gas from the cathode compartment went through the sampling loop of a gas chromatograph (GC9720P, Fuli) and was analysed on line. H_2 was analysed with a thermal conductivity detector; CO, methane and ethylene were analysed with a flame ionization detector; and liquid products (formate, acetate, ethanol and *n*-propanol) were analysed by ^1H NMR spectroscopy (Advance III HD 400-MHz , Bruker). After diluting 0.5 mL of electrolyte solution three times with deionized water, 0.5 mL was taken and mixed with 0.1 mL of DMSO (internal standard, diluted to 25 ppm (v/v) by deuterated water).

The working electrode and counter electrode are carbon paper and Pt wire, and the reference electrode is Ag/AgCl. Linear sweep voltammetry was performed with a scan rate of 50 mV s^{-1} from 0 to −2 V vs. RHE. The EIS measurement was carried out in 1 M KOH solution with an amplitude of 5 mV of 10^{-2} to 10^6 Hz. The electrochemical active surface areas (ECSAs) were determined by measuring double layer capacitance.

ECSAs are proportional to C_{dl} value, which can be obtained from CV curves at different scan rates (20 mV s^{-1}, 40 mV s^{-1}, 60 mV s^{-1}, 80 mV s^{-1}, 100 mV s^{-1}) within the potential range in the absence of the faradaic process. The CV tests were performed in a single cell with three electrodes. The 0.5 M $KHCO_3$ solution was used as the electrolyte.

Evaluation of CO_2RR performance

For gaseous products, the Faradaic efficiency (FE) was calculated as follows.

$$FE = \frac{PV}{T} \times \frac{v \times z \times F \times 10^{-6}(\frac{m^3}{mL})}{Q_{total}}$$

ν (vol %): volume concentration of certain gas product in the exhaust gas from the cell (GC data);

V: gas flow rate measured by a flow meter, 50 mL min^{-1};

Q: the charge passed through the working electrode

z: the electron transfer number for product formation;

F: Faradaic constant, 96485 C mol^{-1};

R: universal gas constant, 8.314 J mol^{-1} K^{-1};

P: one atmosphere, 1.013×10^5 Pa;

T: room temperature, 298.15 K;

FE: faradaic efficiency for H_2, CO, CH_4, C_2H_4 production.

For liquid products, the following method was used for the calculation of FE.

$$FE = \frac{FN}{It} \times \frac{V_i}{V} \times \frac{c_i \cdot N_{Hi}}{N_H}$$

I: total steady-state cell current;

N: the electron transfer number for product formation;

F: Faradaic constant, 96485 C mol^{-1}

V_i: the volume of the catholyte

V: the volume of undiluted cathode liquid in a nuclear magnetic tube

c_i: the concentration of the product *i* in the catholyte gained by NMR

N_{Hi}: the number of H's integrated in the product

N_H: the number of H in DMSO

FE: faradaic efficiency for formate, acetate, ethanol and *n*-propanol production.

The formation rate (R) for each species was calculated using the following equation:

$R = (Q_{tot} \times FE)/(96485 \times z \times t \times S)$

t: the electrolysis time (h)

S: the geometric area of the electrode (cm^2).

Catalysts Characterization

The scanning electron microscope (SEM) images were reflected by ULTRA 55 SEM at 200 K. Transmission electron microscopy (TEM) images of samples were obtained to characterize the sizes and morphologies of on a Hitachi H-800 TEM. X-ray powder diffractometer (XRD) (Rigaku RU-200b with Cu Kα radiation (λ = 1.5406 Å) was performed to confirm the crystalline structure and phase purity. The X-ray photoelectron spectroscopy (XPS) data were recorded using a ULVAC PHI Quantera microscope. Raman measurements were carried out using a Horiba LabRAM HR Evolution Raman microscope. 532 nm He–Ne laser was used as the excitation source.

In-situ ATR-SEIRAS measurement

The in-situ attenuated total reflection-surface-enhanced IR absorption spectroscopy (ATR-SEIRAS) spectroscopy experiments were conducted in a modified electrochemical cell that integrated into a Nicolet iS50 FT-IR spectrometer equipped with mercury-cadmium-telluride (MCT) detector cooled by liquid nitrogen.

During the test 0.5 M $KHCO_3$ was used as electrolyte, Pt wire and Ag/AgCl electrode were used as counter electrode and reference electrode. The working electrode was prepared in two processes. Firstly, a thin film of Au was chemically deposited on the surface of a hemispherical silicon crystal, which can be used as an element for electron transfer to the substrate and IR signal enhancement. Cyclic voltammetry tests were performed on the Au film-loaded silicon crystals at a sweep rate of 100 mV s^{-1} under

0.1 M $HClO_4$ as the electrolyte to remove the surface oxides. Then, a drop of catalyst ink was added to the silicon crystals loaded with Au film by pipetting gun. (Consistent with the ink method for CO_2RR configured electrodes, except that the loading amount was changed to 0.1 mg cm^{-2}).

Prior to in situ ATR-SEIRAS, 0.5 M $KHCO_3$ electrolyte was bubbled with CO_2 for 30 min until saturation. The FTIR chamber and light path were continuously purified with approximately 6 L min^{-1} and 1 L min^{-1} of Ar, respectively. All spectra were expressed in absorbance units log (I/I_0), where I and I_0 denote the sample and reference spectra, respectively. The spectral resolution of all measurements was 8 cm^{-1}. each spectrum was a superposition of 32 interferograms with an acquisition period of 25 s for each spectrum.

In-situ Raman measurement

Raman spectroscopy was recorded using a Raman microscope system (Horiba, Japan) at room temperature. 785 nm using a He-Ne laser as the excitation source. During electrochemical measurements, a panoramic illumination microscope with a water-immersion objective was used to focus and collect the incident and scattered laser light. An optically transparent Teflon film (13 μm thick) was used to cover and protect the objective lens from corrosive electrolytes. The backscattered light was filtered through an edge filter and directed to a regenerative spectrometer (iHR320)/charge-coupled device detector (Synapse CCD). All electrolytes were purged with CO_2 gas for over 3 min prior to in situ Raman spectroscopy measurements. The CO_2 flow rate was set to 20 sccm using a Brooks GF40 mass flow controller. The electrolyte is 1M KOH.

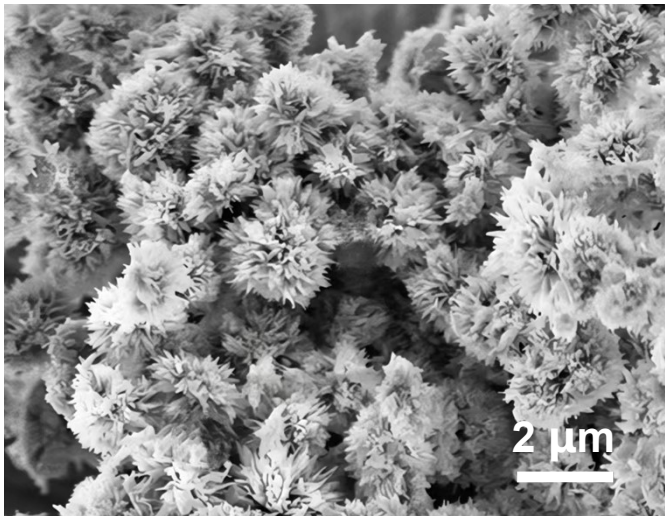

Figure S1. SEM image of CuO nanoflowers.

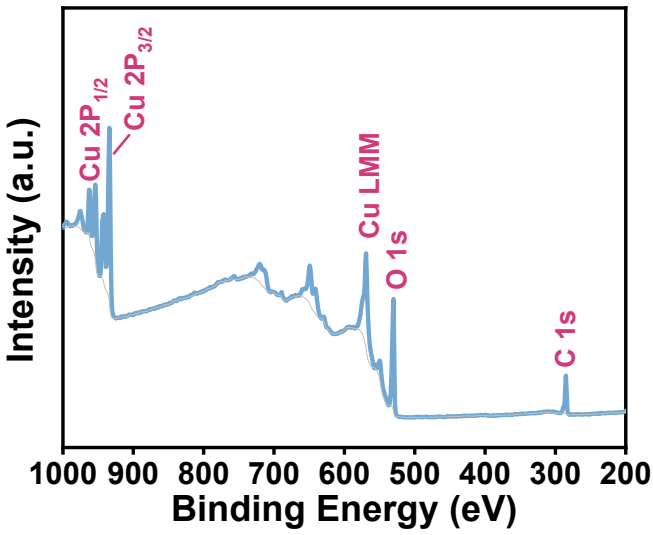

Figure S2. XPS survey spectrum of CuO nanoflowers.

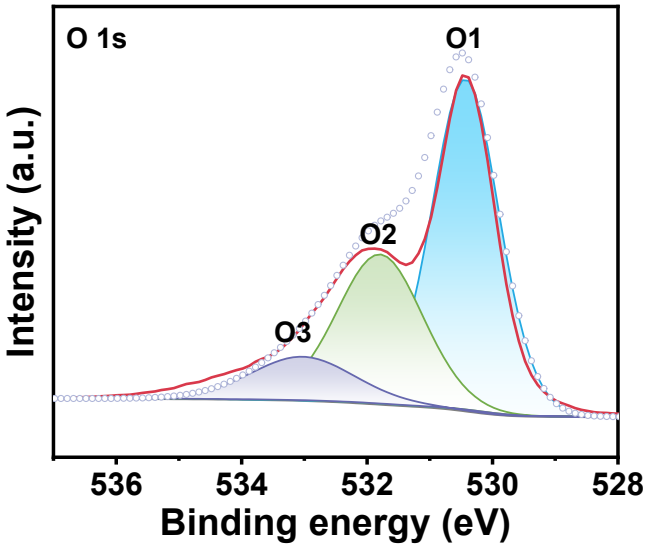

Figure S3. O 1s spectra of CuO nanoflowers.

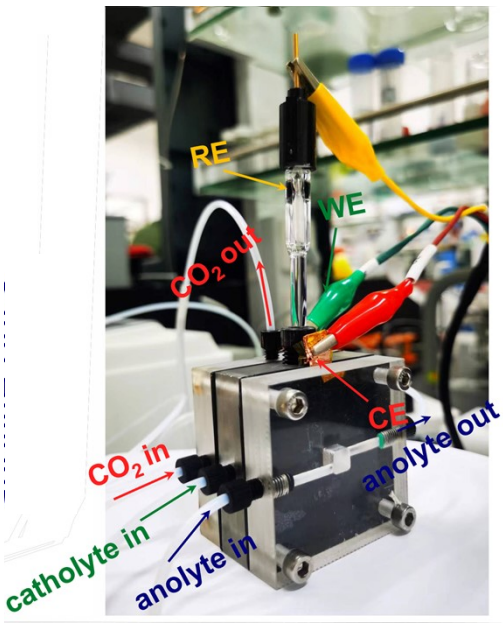

Figure S4. Image of the home-made flow cell employed for CO_2 electrolysis study.

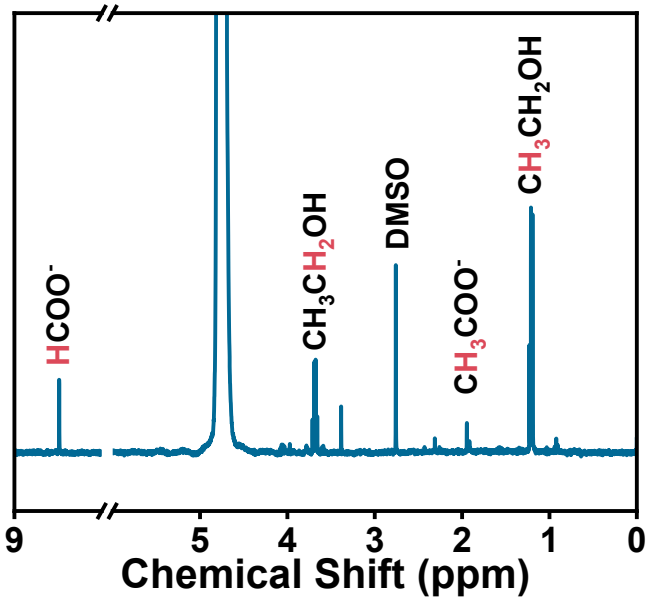

Figure S5. ^{1}H NMR of CuO nanoflowers at a current density of 200 mA cm^{-2}.

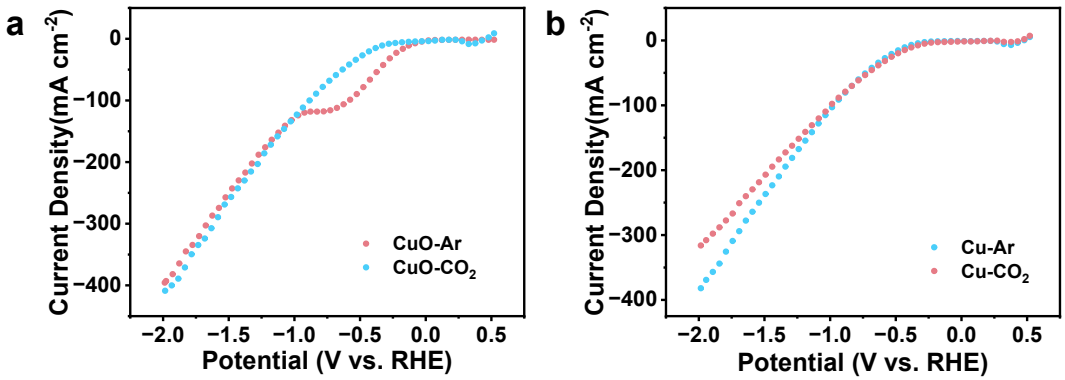

Figure S6. LSV curves in a flow cell of 1 M KOH in (a) CuO nanoflower catalysts and (b) Cu NPs under Ar and CO_2 conditions, respectively.

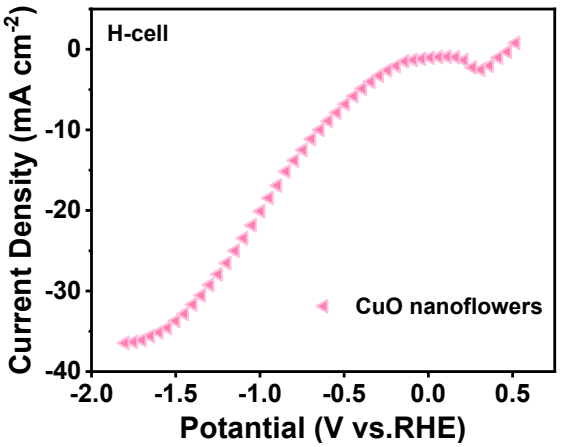

Figure S7. LSV curves of nanoflowers in a H-cell of 1.0 M $KHCO_3$.

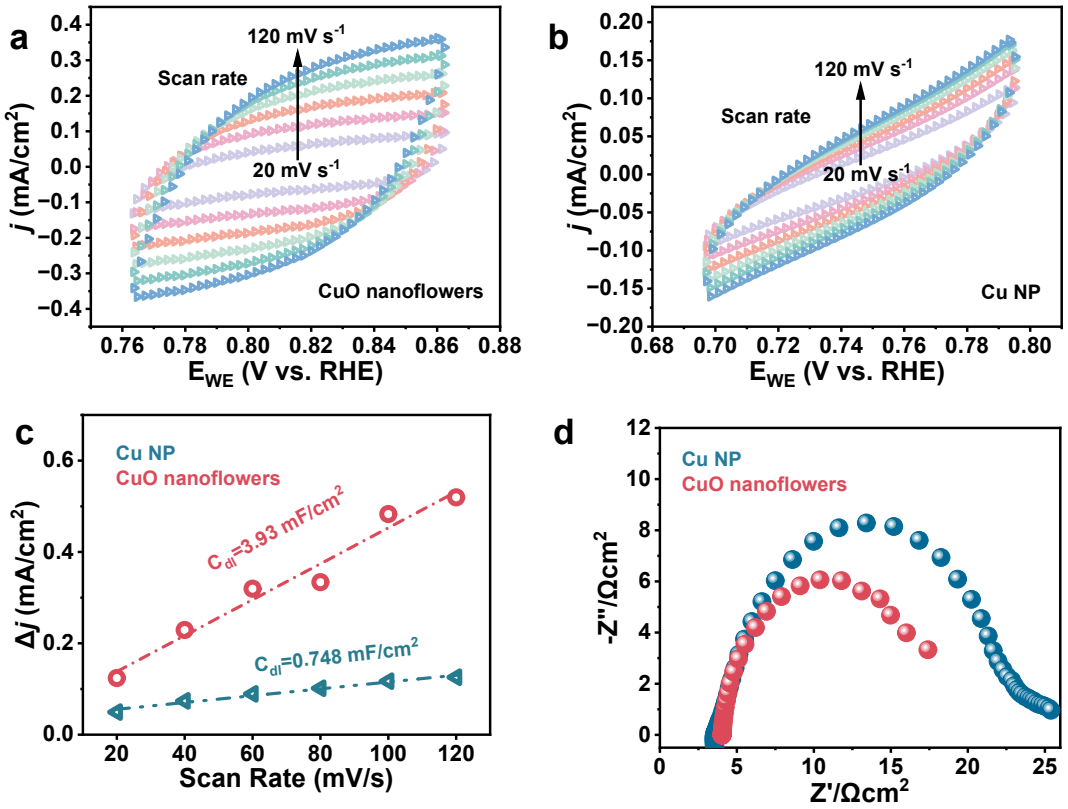

Figure S8. (a-b) The electrochemical active specific surface area (ECSA) on the cathode measurements of CuO nanoflowers and Cu NPs. (c) The measured double-layer capacitance for the as-prepared catalysts. (d) EIS of the as-prepared catalysts in 1 M KOH electrolyte.

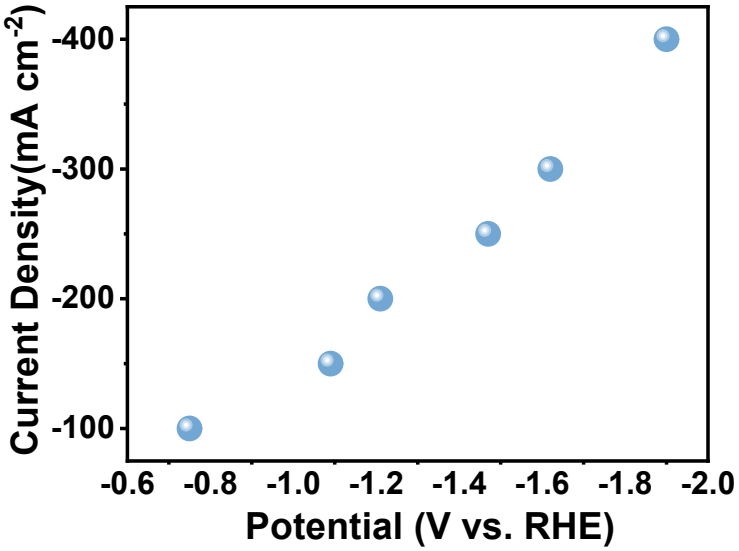

Figure S9. Potential corresponding to CO_2RR test current density.

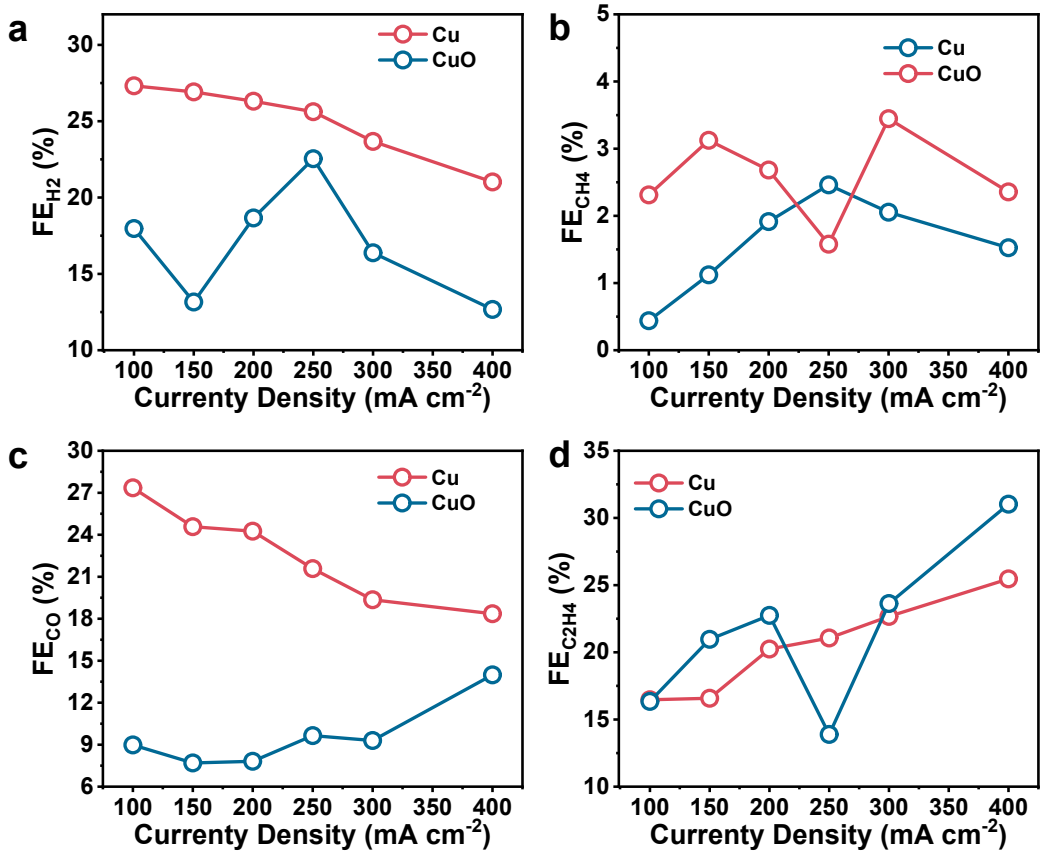

Figure S10. FE of the gas products of CuO nanoflowers and Cu NPs for CO_2RR. (a) FE_{H2}, (b) FE_{CH4}, (c) FE_{CO} and (d) FE_{C2H4}.

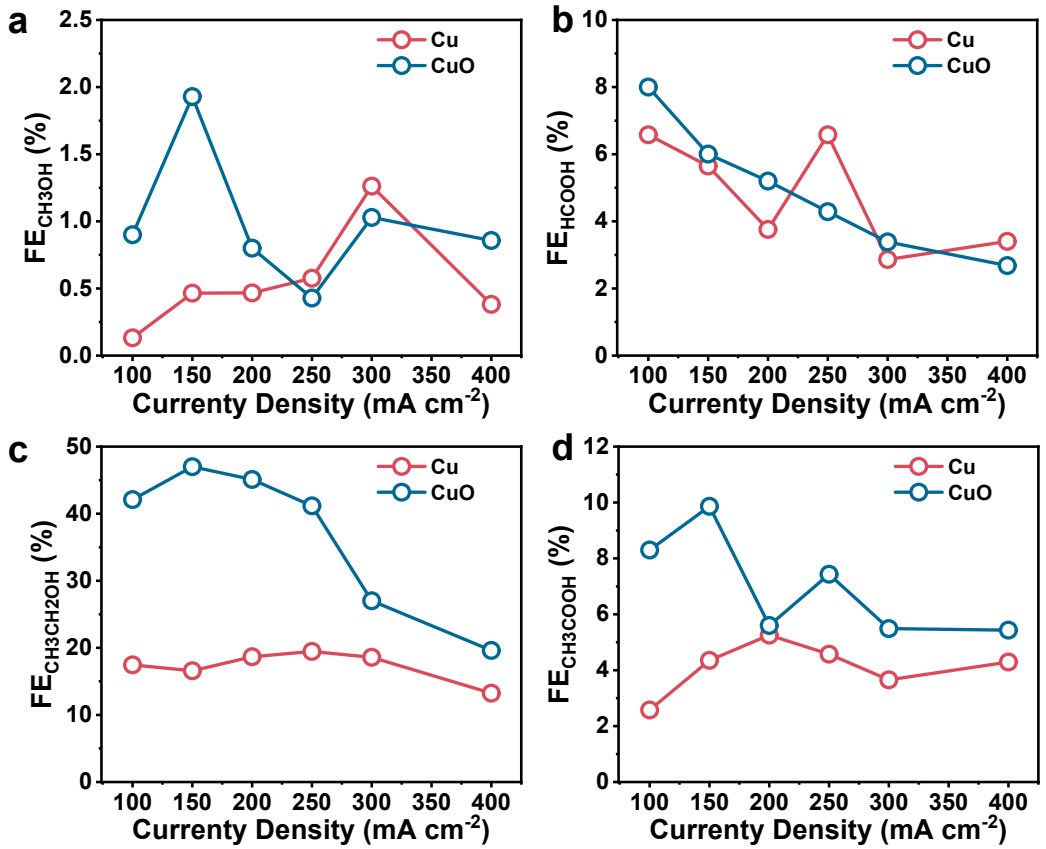

Figure S11. FE of liquid products of CuO nanoflowers and Cu NPs for CO_2RR (a) FE_{CH3OH}, (b) FE_{HCOOH}, (c) FE_{C2H5OH} and(d) $FE_{CH3COOH}$.

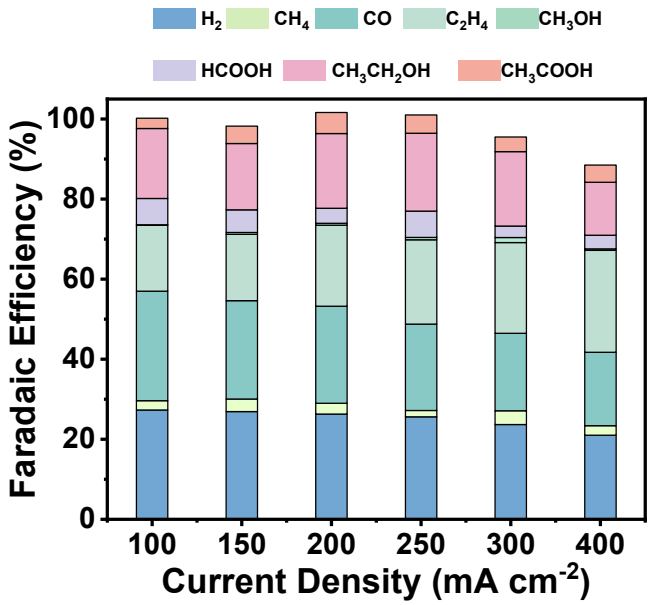

Figure S12. FE of each product of Cu NPs for CO_2RR.

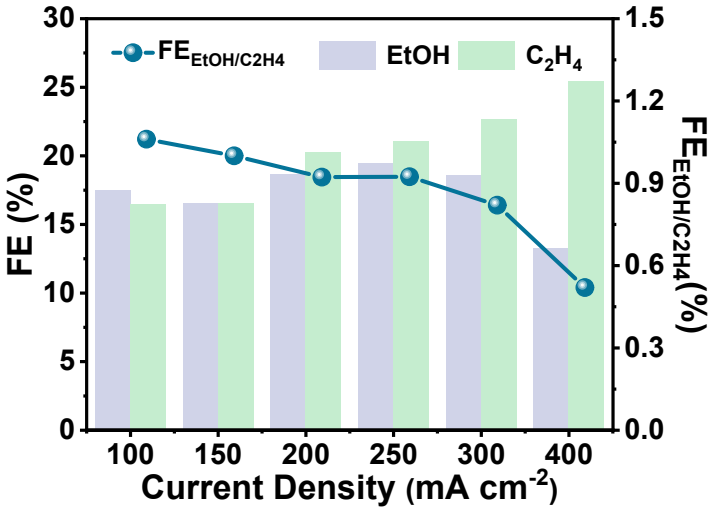

Figure S13. Ratio of FE_{EtOH} to FE_{C2H4} and distribution of C_2H_4 and EtOH of CuNPs.

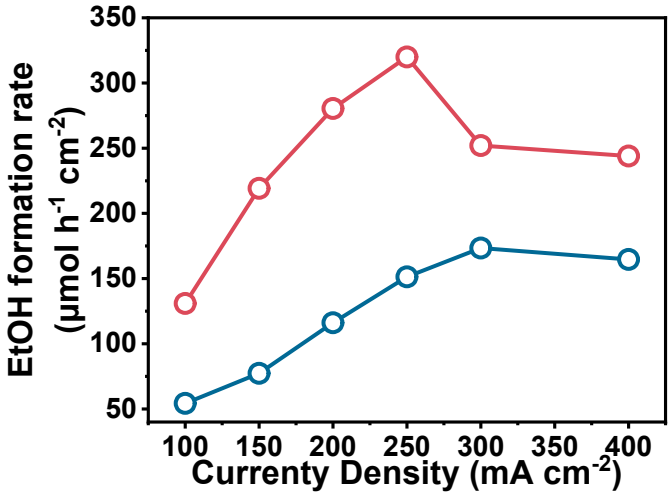

Figure S14. Ethanol formation rates of CuO nanoflowers and Cu NPs.

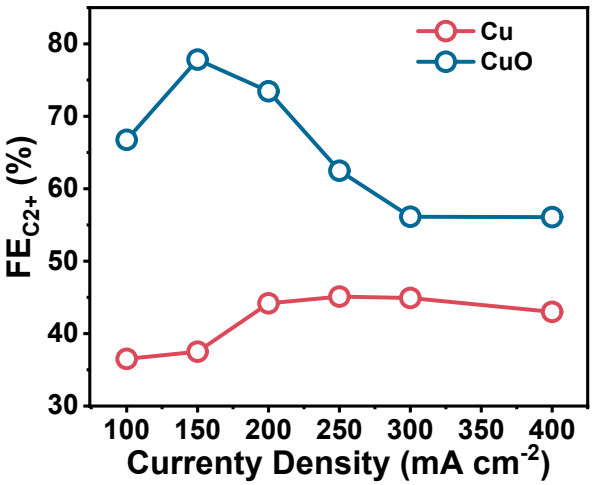

Figure S15. FE_{C2+} of CuO nanoflowers and Cu NPs for CO_2RR.

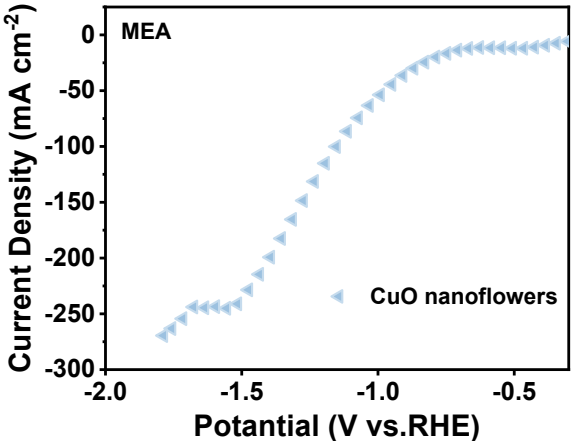

Figure S16. LSV curves of nanoflowers in a MEA in 1.0 M KOH.

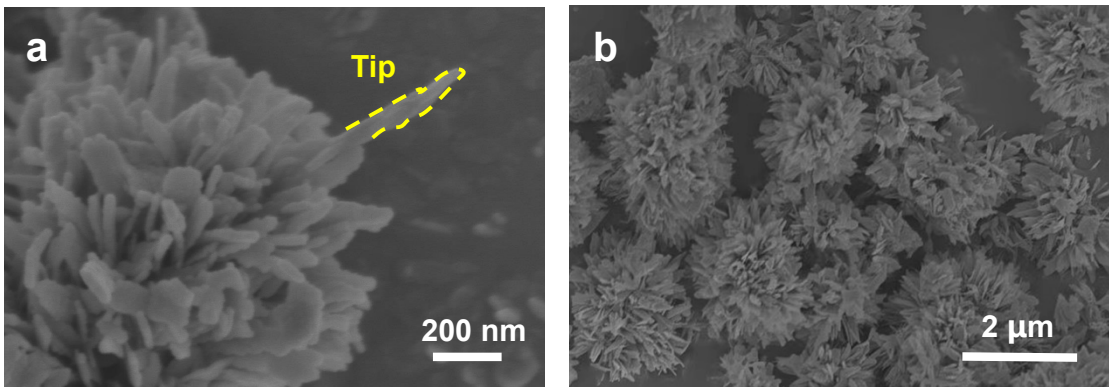

Figure S17. CuO nanoflowers image of SEM after undergoing stability testing.

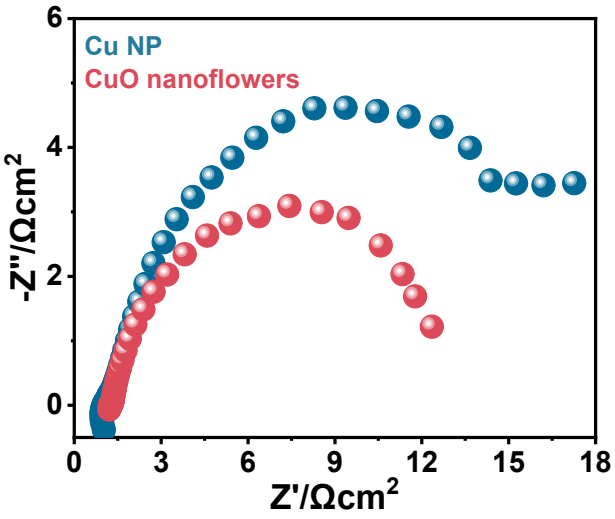

Figure S18. EIS of the prepared catalyst after undergoing stability testing.

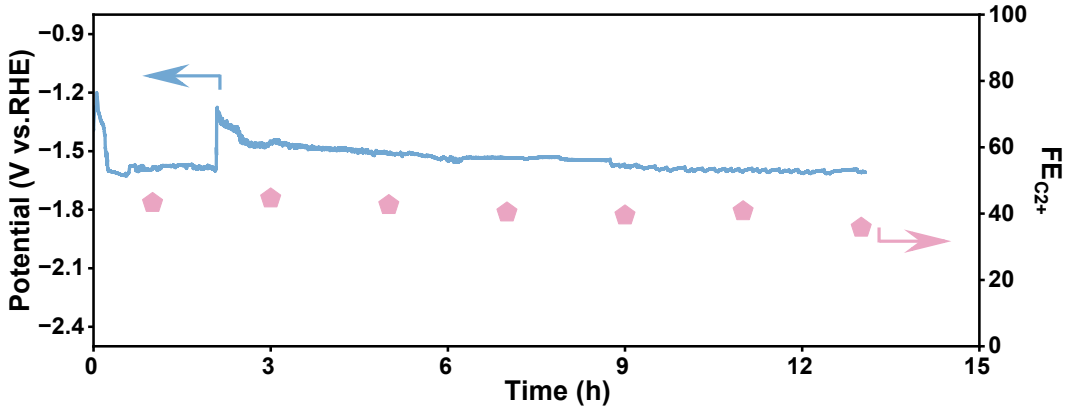

Figure S19. Long-term stability of Cu NPs electrode at 100 $mAcm^{-2}$.

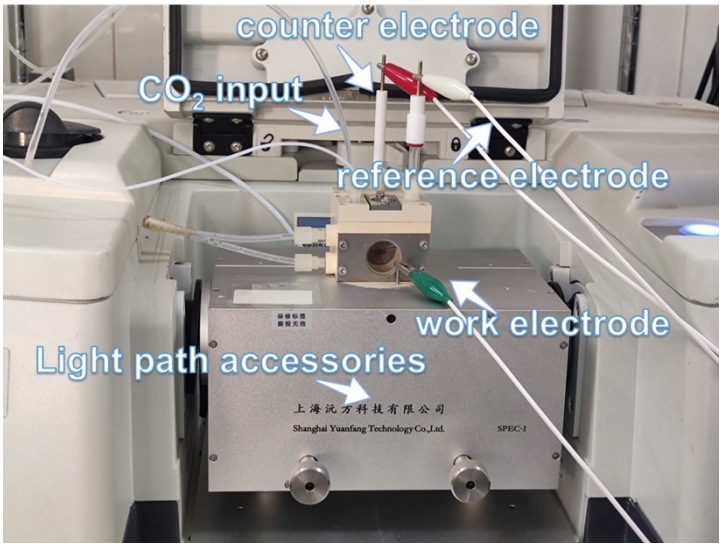

Figure S20. Optical photograph of the in situ ATR-SEIRAS test setup and the customized electrochemical cell.

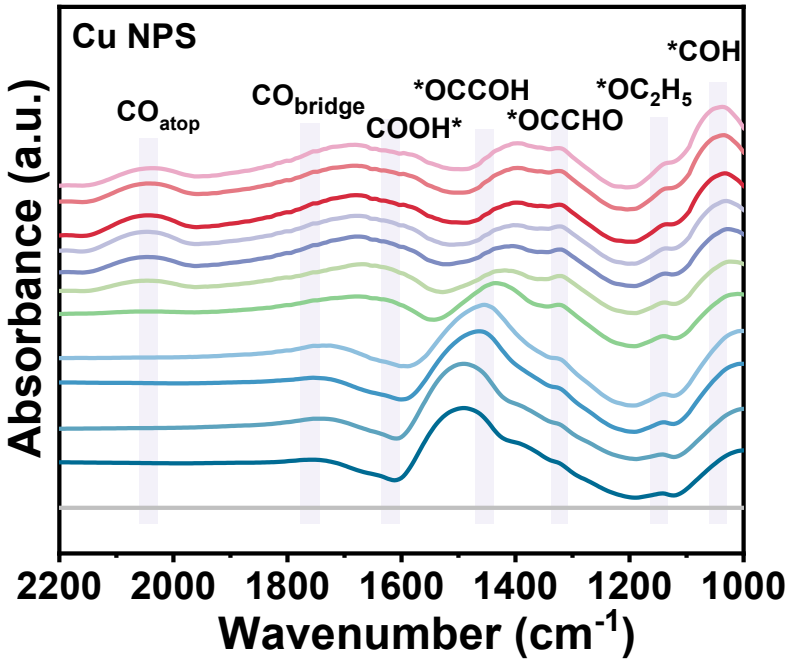

Figure S21. In situ ATR-SEIRAS measurements of Cu NPs.

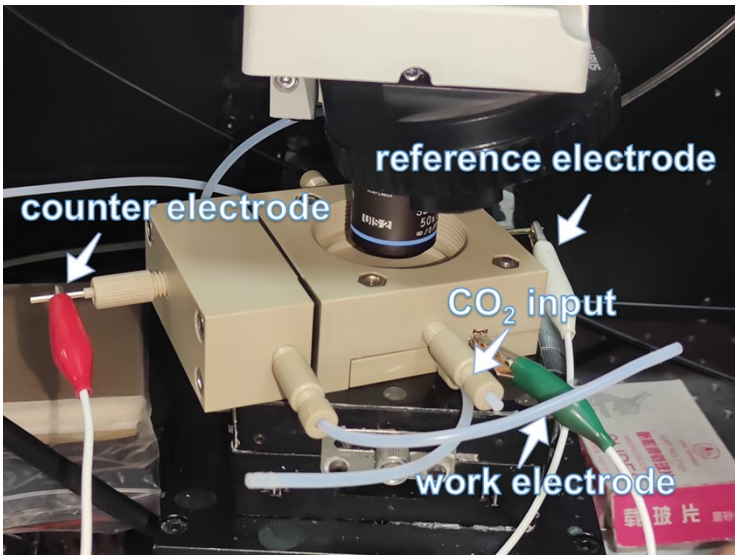

Figure S22. Optical photograph of the in situ Raman test setup and the customized electrochemical cell.

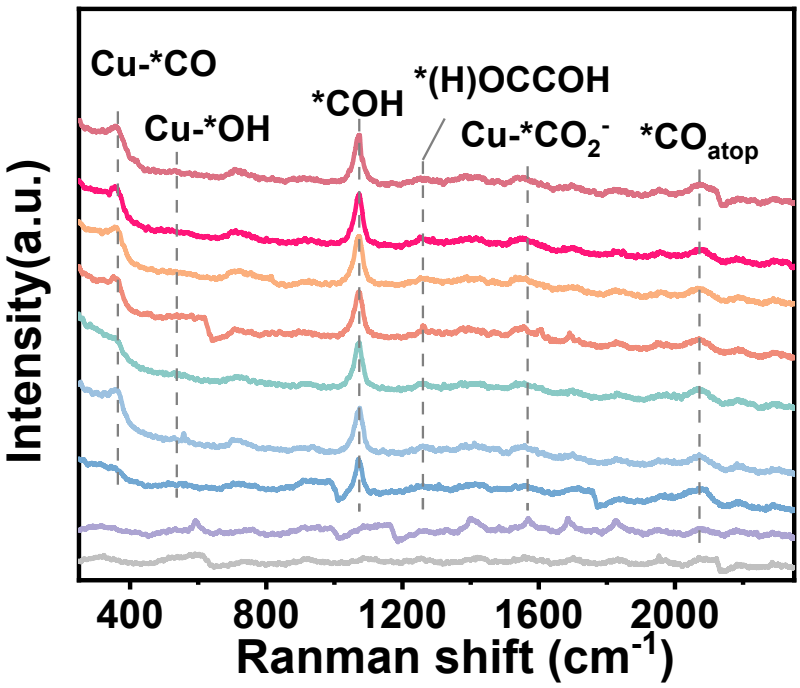

Figure S23. In situ Raman spectra for adsorbed intermediates on Cu NPs.

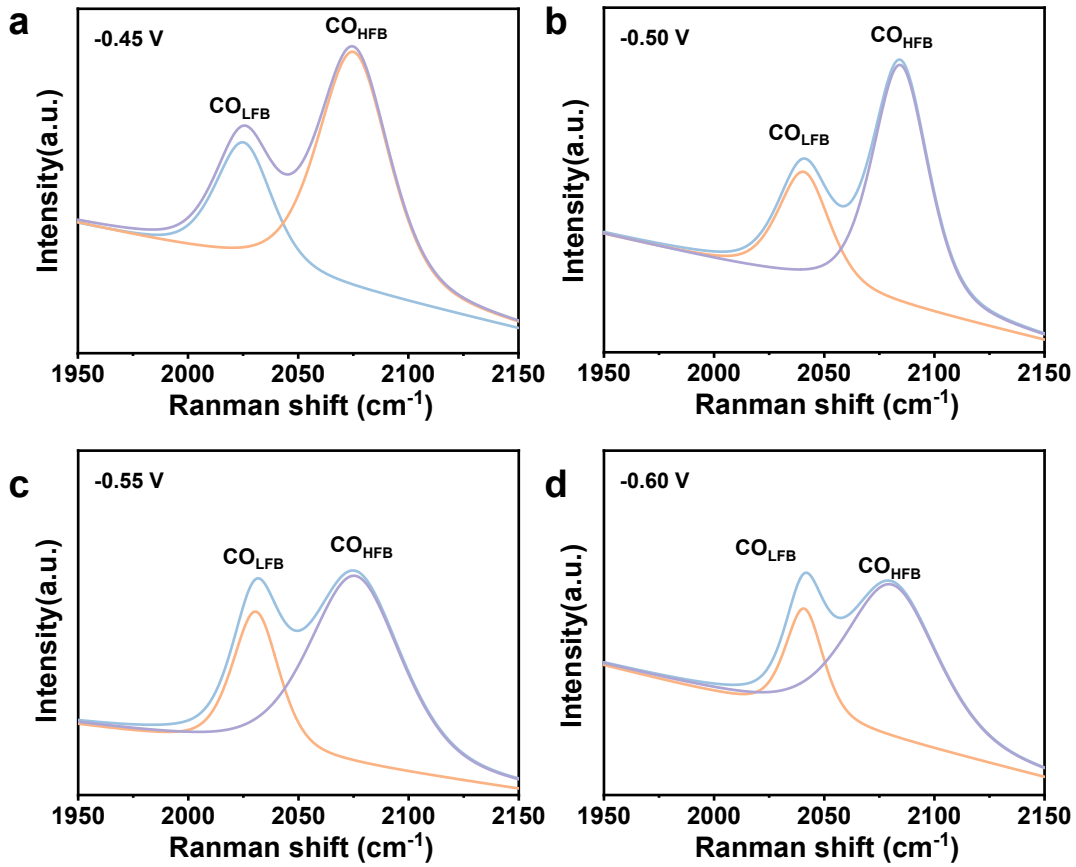

Figure S24. Representative in situ Raman spectra showing the decomposition of $^{*}CO$ intermediates adsorbed on CuO nanoflowers to $^{*}CO_{LFB}$ and $^{*}CO_{HFB}$ at -0.45 to -0.6 V_{RHE}.

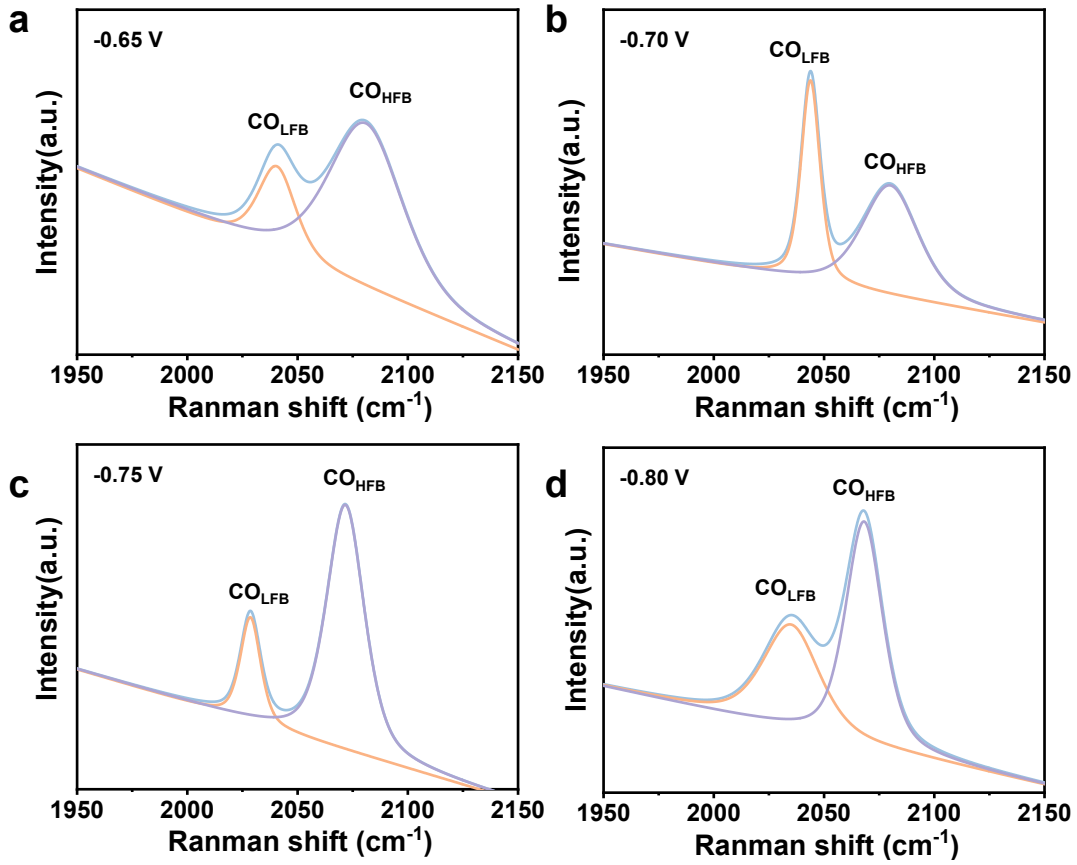

Figure S25. Representative in situ Raman spectra showing the decomposition of *CO intermediates adsorbed on CuO nanoflowers to $^{*}CO_{LFB}$ and $^{*}CO_{HFB}$ at -0.65 to -0.80 V_{RHE}.

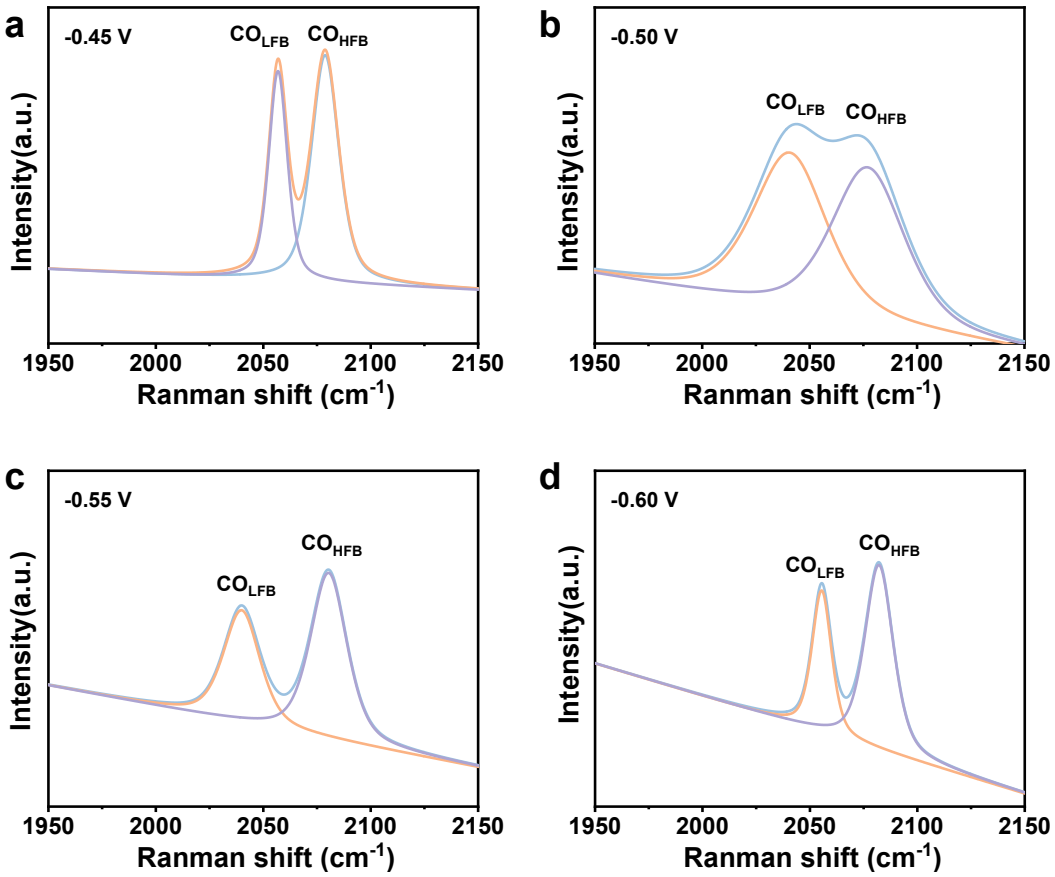

Figure S26. Representative in situ Raman spectra showing the decomposition of *CO intermediates adsorbed on Cu NPs to $^{*}CO_{LFB}$ and $^{*}CO_{HFB}$ at -0.45 to -0.60 V_{RHE}.

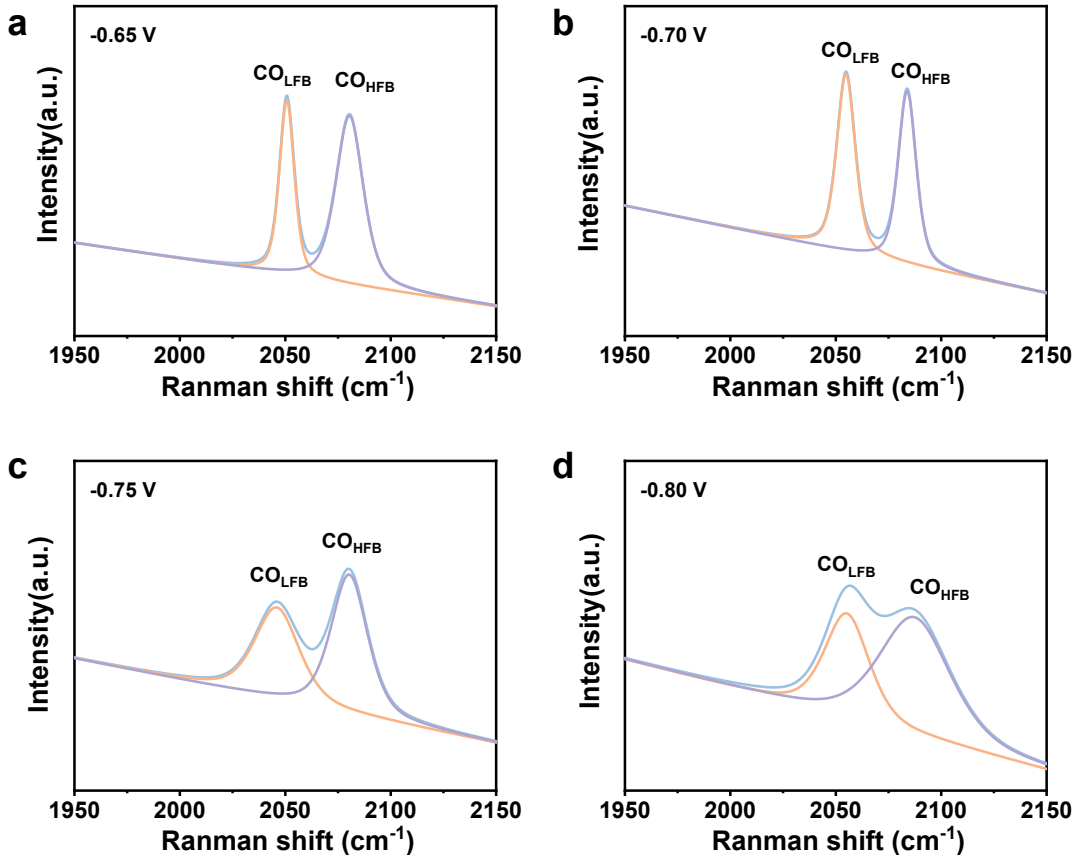

Figure S27. Representative in situ Raman spectra showing the decomposition of *CO intermediates adsorbed on Cu NPs to $^{*}CO_{LFB}$ and $^{*}CO_{HFB}$ at -0.65 to -0.80 V_{RHE}.

Table 1. The C_{dl} and ECSA values of Cu NPs and CuO nanoflowers.

Catalysts	C_{dl}(mF cm^{-2})	R_f[a]	ECSA[b](cm^2)
Cu NPs	0.748	25.79	25.79
CuO nanoflowers	3.93	135.52	135.52

[a] R_f was estimated from the ratio of double-layer capacitance (C_{dl}) for the working electrode and the corresponding smooth polycrystalline Cu electrode (29 μF cm^{-2}). [b] ECSA = R_f × S, where S stands for the geometric area of the electrode (in this work, S = 1 cm^2).